New Journal and we have not received input yet 33 (2022) 101346

Contents lists available at ScienceDirect

Thermal Science and Engineering Progress

journal homepage: www.sciencedirect.com/journal/thermal-science-and-engineering-progress

Prediction of activation energy for combustion and pyrolysis by means of machine learning

Furkan Kartal, Uğur Özveren *

Department of Chemical Engineering, Marmara University, Goztepe Campus, 34722, Kadikoy, Turkey

ARTICLE INFO

Keywords:
Machine learning
ANN
Activation energy
Fuel properties
Pyrolysis
Combustion

ABSTRACT

Thermogravimetric analysis (TGA) is a widely used technique to determine the activation energy (Ea), which is an important parameter for thermochemical processes. Thus, researchers have recently developed computational methods to minimize the experimental effort. While there are some studies on estimating kinetic parameters such as Ea using artificial neural networks (ANN), these are insufficient for generalization because they involve only one or two operational parameters. Therefore, in this study, Ea estimation was performed by creating a realistic ANN model as a machine learning approach, including operating parameters that were not previously considered. TGA experiments were performed with biomass, coal, and blends under different operating conditions for the training and test data sets of the model. In order for the ANN to give a satisfactory result, the experimental results were enriched with the data from the literature. The dataset was analyzed using statistical tools like correlation map, feature importance etc. Then a feedforward neural network was developed using Levenberg-Marquardt optimization algorithm.

As a result, by using an appropriate number of input variables and a sufficient amount of data, it was possible to conduct a reliable TGA simulation to calculate the Ea values, with R^2 values greater than 0.96 and mean absolute percentage error values<20%. Furthermore, the results of the statistical analysis applied to the input parameters of the ANN model were found to be consistent with the scientific background. The initial and final temperatures of decomposition are the most significant parameters for the determination of Ea.

Introduction

Fossil fuel depletion has increased in the last century as a result of rapid industrialization and population growth. Coal is the preferred solid fuel for power generation due to its large reserves and high calorific value compared to other solid fuels [1]. Although it is a valuable solid fuel, the use of coal has several negative impacts on human and environmental health. The demand of the world's population for large amounts of energy has led to the need to adopt more environmentally friendly and efficient methods [2–3]. Therefore, in our modern life, a considerable amount of energy demand is met by non-renewable energy sources [4]. Biomass is abundant and tremendously diverse. Biomass contributes less to greenhouse gases than fossil fuels and offers an alternative because of its carbon neutrality and abundance [5]. However, biomass has low calorific value and high moisture content compared to coal [6–7]. Therefore, the utilization of biomass in current power plants only covers a smaller part of our energy needs.

Thermochemical processes (combustion, pyrolysis, and gasification) are critical to the use of solid fuels, both in their use as primary energy sources and in their conversion into beneficial chemicals with different cycles. Combustion is a more mature technology than gasification and pyrolysis, and its efficiency is also higher in combined heat and power systems [8]. Unlike combustion, pyrolysis is a thermal decomposition process that is applied to obtain solid, liquid, and gaseous products under an inert atmosphere. One of the advantages of pyrolysis is that a wide variety of chemicals can be produced depending on the flexible operating conditions [9]. Moreover, pyrolysis is also a common step for other thermochemical conversions, and understanding the pyrolysis mechanics is important for acknowledging other steps [10]. Thermodynamic and kinetic mechanisms need to be investigated to make pyrolysis a more mature process on a commercial scale. Similarly, the derivation of combustion kinetics for the generation of boilers, furnaces and powders at industrial scale is necessary [11].

Activation energy (Ea) is an important kinetic parameter in determining the ranking of reactions, products, and mechanisms [12]. Although reliable techniques such as quantum chemical methods are

* Corresponding author.
E-mail address: ugur.ozveren@marmara.edu.tr (U. Özveren).

https://doi.org/10.1016/j.tsep.2022.101346
Received 18 September 2021; Received in revised form 17 May 2022; Accepted 17 May 2022
Available online 20 May 2022

Table 1
Comparison of the study with the literature for the prediction of kinetic parameters.

	Çepelioğullar et al. (9)	Sunphorka et al. [29]	Jiang et al. [30]	This study
Methodology	TGA - ANN	Data collection - ANN	TGA – Different machine learning tools	TGA/Data collection - ANN
Fuel(s)	Lignocellulosic forest residue and olive oil residue	Biomass and waste	Wheat straw, corn straw and sorghum straw, KOH and NaOH catalyzed straw pyrolytic carbon	Biomass, municipal wastes/sludges, polymers, lignites, and various blends
Atmosphere	Nitrogen	Oxidative	Air atmosphere	Argon and Air atmosphere
Input	Temperature. Heating rate (5, 10, 20 and 50 °C/min)	FC, VM, Ash, O_2 concentration, ER	–	C, H, O, Temperature Range, Heating Rate, Flow Rate, Particle Size, Atmosphere
Output	Weight loss (%)	Kinetic triplets	Activation energy	Activation energy
Study	The authors calculated the activation energy using the model-free approach (experimentally) and using the output variable of ANN. They developed the optimum ANN model based on the relative error between experimental and predicted activation energies.	The authors developed the ANN model using data from the literature and predicted the kinetic triplets for only combustion reactions.	The authors performed combustion experiments and calculated the activation energy by using distributed modified Coats-Redfern integration method.	For the first time, the effects of particle size, flow rate and two different atmospheres were evaluated for a wide range of solid fuels. The activation energy was forecasted considering the Coats-Redfern first order integral method.

Table 2
Proximate and ultimate analysis results of the feedstock materials.

	Almond Shell	İmbat Coal
Moisture (wt %, ar.)	2.27	5.62
Fixed Carbon (wt %, ar.)	20.02	46.68
Volatile Matter (wt %, ar.)	76.51	32.89
Ash (wt %, ar.)	1.20	14.81
C (wt %, daf.)	45.72	64.67
H (wt %, daf.)	5.80	5.41
O (wt %, daf.)	45.26	25.64
N (wt %, daf.)	0.15	1.34
S (wt %, daf.)	3.08	2.93

used to measure Ea, they are inadequate for complex processes involving many reactions and require excessive computational cost [13]. Thermogravimetric analysis (TGA) is one of the most preferred methods to investigate thermochemical conversions [14], and TGA is employed to calculate the pre-exponential factor, Ea, and the reaction model for solid fuels. Kinetic parameters are derived by applying quantitative methods to TG curves. Coats-Redfern (first-order reaction), one of the conventional methods, is used in TGA experiments to calculate kinetic parameters by many researchers [15–18]. Furthermore, the type of solid fuel and operational parameters have an undeniable impact on the results of this kinetic triplet. The characteristics of thermal decomposition and hence the Ea value are inextricably linked to the elemental composition of the fuel, e.g. oxygen/carbon (O/C) and hydrogen/carbon (H/C) [19]. Additionally, the temperature range of the thermolysis process has a significant effect on the kinetic parameters, as complex structures in heterogeneous solid fuels are degraded at different temperatures [20]. Since the particle size and heating rate (HR) affect the mass loss rate, the mechanics of heat/mass transfer, and consequently the reaction pathways, they have a considerable impact on the thermal degradation of feedstock material [21–22].

The development of computer-based approaches to reduce the number of laboratory experiments is becoming increasingly popular. Recently, machine learning has played an important role in the development of algorithms for a variety of scientific fields - including chemistry [23–24]. Artificial neural networks (ANNs), a subtype of machine learning, can establish correlations between input and output for nonlinear relationships, complicated tasks, and large data sets [25]. Therefore, ANNs have been used by many authors to estimate the parameters in the process of decomposition of solid fuels [26–28] including the determination of kinetic parameters. Table 1 summarizes the studies that were previously reported in the literature for kinetic parameter estimation.

The aim of this study is to estimate the activation energy for pyrolytic and oxidative atmosphere without using complex equations and instruments. Unlike similar studies in the literature, this study considers for the first time the influence of particle size and evaluates the flow rate (FR) and temperature ranges for different stages of the thermolysis process. Therefore, the aim is to develop a more realistic kinetic prediction for solid fuel thermolysis. Experimental procedures were performed to generate data for the ANN model. In addition, various thermogravimetric analysis results were collected from the literature so as not to be dependent on a particular fuel type and operating conditions. The Ea values were determined using the Coats-Redfern method in both the experimental study and the literature. Several statistical analyses of the generated data set were also performed and the frequency distribution of the input parameters, their relative importance and correlations with each other, and the relationship between the statistical results and the scientific justification were discussed. Thus, statistical analyses were also performed to find an answer to the question of whether the activation energy can be determined using the ANN model developed in this study without experimental TGA procedures and complex equations.

Methodology

Raw material Collection, Preparation, and characterization

The feedstock materials used in this study were supplied from local farmers in the Aegean region, Turkey, and the Turkish Coal Enterprises Institution. Before the TGA procedure, the samples were dried at 105 °C for 24 h, further, milled and sieved under 250 μm. The shredder "IKA M20 Universal Mill" was used to reduce the size of the almond shell, and Imbat coal samples were ground via "Mortar Grinder Retsch RM 200". ASTM Standard Test Methods (ASTM Standard D 5142–04) for proximate analysis were employed to determine the weight fractions of ash, moisture, fixed carbon (FC), and volatile matter (VM) contents via the "Netzsch 409 PC Luxx" thermogravimetric analyzer. Ultimate analysis experiments were performed with the test method of ASTM Standard D5373-2 standards in Advanced Technologies Application and Research Center, Hacettepe University. Ultimate analyses of the Imbat coal and almond shell samples were carried out with the LECO brand Truspec micro elemental analyzer. Table 2 summarizes the proximate and ultimate analysis of the feedstock materials.

The Imbat coal possesses the higher content of FC and ash and the lower amount of VM compared to almond shell. Furthermore, the higher H/C and O/C ratio appear for the almond shell when the ultimate analysis results were examined. In contrast, Imbat coal depicts opposite physicochemical properties as mentioned in the Van Krevelen diagram [31].

Table 3
The ultimate analysis properties of the fuels and the experimental TGA results of these fuels used for the ANN model.

Sample	C (wt. %)	H (wt. %)	O (wt. %)	Thermolysis	TI (°C)	TF (°C)	HR (°C/min)	FR (ml/min)	Particle Size (μm)	Ea (kJ/mol)	Ref.
Rice husk	50.10	5.33	43.77	Pyrolysis	269.2	351.7	5	100	120–150	64.33	[36]
Straw	49.08	5.76	43.99	Pyrolysis	246.2	341.6	5	100	120–150	49.35	
Pine	60.28	5.73	33.75	Pyrolysis	290.1	367.8	5	100	120–150	63.69	
Pine nut shell	52.89	5.98	40.55	Pyrolysis	264.5	352.0	5	100	120–150	58.98	
Rice husk	50.10	5.33	43.77	Pyrolysis	276.7	364.2	10	100	120–150	62.92	
Straw	49.08	5.76	43.99	Pyrolysis	258.7	351.4	10	100	120–150	51.67	
Pine	60.28	5.73	33.75	Pyrolysis	295.1	380.4	10	100	120–150	63.82	
Pine nut shell	52.89	5.98	40.55	Pyrolysis	274.5	364.5	10	100	120–150	57.60	
Rice husk	50.10	5.33	43.77	Pyrolysis	284.2	376.7	20	100	120–150	61.91	
Straw	49.08	5.76	43.99	Pyrolysis	268.8	366.4	20	100	120–150	51.59	
Pine	60.28	5.73	33.75	Pyrolysis	310.2	395.4	20	100	120–150	66.09	
Pine nut shell	52.89	5.98	40.55	Pyrolysis	279.5	377.0	20	100	120–150	57.33	
Rice husk	50.10	5.33	43.77	Pyrolysis	299.2	389.2	40	100	120–150	65.31	
Straw	49.08	5.76	43.99	Pyrolysis	273.8	376.4	40	100	120–150	49.86	
Pine	60.28	5.73	33.75	Pyrolysis	322.7	407.9	40	100	120–150	65.32	
Pine nut shell	52.89	5.98	40.55	Pyrolysis	297.0	389.5	40	100	120–150	62.02	
Walnut shell	47.50	6.39	45.65	Pyrolysis	208.0	365.0	5	20	425–600	102.31	[37]
Walnut shell	47.50	6.39	45.65	Pyrolysis	215.0	370.0	10	20	425–600	109.83	
Walnut shell	47.50	6.39	45.65	Pyrolysis	230.0	410.0	15	20	425–600	97.51	
Walnut shell	47.50	6.39	45.65	Pyrolysis	232.0	415.0	20	20	425–600	89.78	
Walnut shell	47.50	6.39	45.65	Pyrolysis	248.0	440.0	50	20	425–600	108.45	
Cotton stalk	47.95	5.50	43.31	Pyrolysis	42.0	102.0	10	100	< 250	67.42	[15]
Cotton stalk	47.95	5.50	43.31	Pyrolysis	107.0	202.0	10	100	< 250	38.90	
Cotton stalk	47.95	5.50	43.31	Pyrolysis	207.0	382.0	10	100	< 250	79.48	
Hazelnut shell	56.37	5.62	32.05	Pyrolysis	28.0	108.0	10	100	< 250	62.81	
Hazelnut shell	56.37	5.62	32.05	Pyrolysis	113.0	203.0	10	100	< 250	38.53	
Hazelnut shell	56.37	5.62	32.05	Pyrolysis	208.0	383.0	10	100	< 250	82.45	
Sunflower residue	47.91	5.27	38.17	Pyrolysis	37.0	77.0	10	100	< 250	72.67	
Sunflower residue	47.91	5.27	38.17	Pyrolysis	82.0	192.0	10	100	< 250	30.64	
Sunflower residue	47.91	5.27	38.17	Pyrolysis	197.0	362.0	10	100	< 250	74.20	
E. rigida	54.17	5.70	38.30	Pyrolysis	39.0	99.0	10	100	< 250	74.66	
E. rigida	54.17	5.70	38.30	Pyrolysis	104.0	224.0	10	100	< 250	36.13	
E. rigida	54.17	5.70	38.30	Pyrolysis	229.0	359.0	10	100	< 250	88.87	
Polyethylene terephthalate	75.21	3.90	16.01	Pyrolysis	373.0	443.0	10	100	< 250	347.40	
Polyethylene terephthalate	75.21	3.90	16.01	Pyrolysis	448.0	503.0	10	100	< 250	172.60	
Polyvinyl chloride	55.98	6.14	37.34	Pyrolysis	222.0	292.0	10	100	< 250	246.78	
Polyvinyl chloride	55.98	6.14	37.34	Pyrolysis	297.0	387.0	10	100	< 250	108.12	
Polyvinyl chloride	55.98	6.14	37.34	Pyrolysis	392.0	522.0	10	100	< 250	191.32	
CS/PET	61.58	4.70	29.66	Pyrolysis	34.0	89.0	10	100	< 250	68.59	
CS/PET	61.58	4.70	29.66	Pyrolysis	94.0	144.0	10	100	< 250	72.95	
CS/PET	61.58	4.70	29.66	Pyrolysis	149.0	214.0	10	100	< 250	76.57	
CS/PET	61.58	4.70	29.66	Pyrolysis	219.0	369.0	10	100	< 250	89.02	
CS/PET	61.58	4.70	29.66	Pyrolysis	374.0	504.0	10	100	< 250	171.48	
HS-PET	65.79	4.76	24.03	Pyrolysis	38.0	88.0	10	100	< 250	73.94	
HS-PET	65.79	4.76	24.03	Pyrolysis	93.0	133.0	10	100	< 250	85.50	
HS-PET	65.79	4.76	24.03	Pyrolysis	138.0	208.0	10	100	< 250	61.79	
HS-PET	65.79	4.76	24.03	Pyrolysis	213.0	348.0	10	100	< 250	93.36	
HS-PET	65.79	4.76	24.03	Pyrolysis	353.0	503.0	10	100	< 250	139.04	
SFR-PET	61.56	4.59	27.09	Pyrolysis	43.0	98.0	10	100	< 250	66.63	
SFR-PET	61.56	4.59	27.09	Pyrolysis	103.0	188.0	10	100	< 250	50.24	
SFR-PET	61.56	4.59	27.09	Pyrolysis	193.0	303.0	10	100	< 250	91.20	
SFR-PET	61.56	4.59	27.09	Pyrolysis	308.0	378.0	10	100	< 250	123.55	
SFR-PET	61.56	4.59	27.09	Pyrolysis	383.0	443.0	10	100	< 250	315.82	
SFR-PET	61.56	4.59	27.09	Pyrolysis	448.0	548.0	10	100	< 250	104.64	
SFR-PET	61.56	4.59	27.09	Pyrolysis	553.0	648.0	10	100	< 250	261.32	
ER-PET	64.69	4.80	27.16	Pyrolysis	42.0	97.0	10	100	< 250	63.36	
ER-PET	64.69	4.80	27.16	Pyrolysis	102.0	177.0	10	100	< 250	52.19	
ER-PET	64.69	4.80	27.16	Pyrolysis	182.0	292.0	10	100	< 250	86.43	
ER-PET	64.69	4.80	27.16	Pyrolysis	297.0	377.0	10	100	< 250	115.28	
ER-PET	64.69	4.80	27.16	Pyrolysis	382.0	447.0	10	100	< 250	277.45	
ER-PET	64.69	4.80	27.16	Pyrolysis	452.0	557.0	10	100	< 250	112.80	
ER-PET	64.69	4.80	27.16	Pyrolysis	562.0	637.0	10	100	< 250	316.34	
CS-PVC	51.97	5.82	40.33	Pyrolysis	67.0	137.0	10	100	< 250	51.08	
CS-PVC	51.97	5.82	40.33	Pyrolysis	142.0	187.0	10	100	< 250	108.82	
CS-PVC	51.97	5.82	40.33	Pyrolysis	192.0	322.0	10	100	< 250	139.11	
CS-PVC	51.97	5.82	40.33	Pyrolysis	327.0	387.0	10	100	< 250	157.78	
CS-PVC	51.97	5.82	40.33	Pyrolysis	392.0	502.0	10	100	< 250	190.13	
HS-PVC	56.18	5.88	34.70	Pyrolysis	38.0	138.0	10	100	< 250	45.06	
HS-PVC	56.18	5.88	34.70	Pyrolysis	143.0	188.0	10	100	< 250	96.31	
HS-PVC	56.18	5.88	34.70	Pyrolysis	193.0	333.0	10	100	< 250	135.99	
HS-PVC	56.18	5.88	34.70	Pyrolysis	338.0	408.0	10	100	< 250	127.17	

(*continued on next page*)

Table 3 (*continued*)

Sample	C (wt. %)	H (wt. %)	O (wt. %)	Thermolysis	TI (°C)	TF (°C)	HR (°C/min)	FR (ml/min)	Particle Size (μm)	Ea (kJ/mol)	Ref.
SFR-PVC	51.95	5.71	37.76	Pyrolysis	33.0	113.0	10	100	< 250	45.88	
SFR-PVC	51.95	5.71	37.76	Pyrolysis	118.0	203.0	10	100	< 250	66.24	
SFR-PVC	51.95	5.71	37.76	Pyrolysis	208.0	293.0	10	100	< 250	146.98	
SFR-PVC	51.95	5.71	37.76	Pyrolysis	298.0	393.0	10	100	< 250	95.05	
SFR-PVC	51.95	5.71	37.76	Pyrolysis	398.0	508.0	10	100	< 250	197.72	
ER-PVC	55.08	5.92	37.82	Pyrolysis	33.0	113.0	10	100	< 250	42.10	
ER-PVC	55.08	5.92	37.82	Pyrolysis	118.0	193.0	10	100	< 250	65.41	
ER-PVC	55.08	5.92	37.82	Pyrolysis	198.0	328.0	10	100	< 250	113.41	
ER-PVC	55.08	5.92	37.82	Pyrolysis	333.0	408.0	10	100	< 250	135.46	
ER-PVC	55.08	5.92	37.82	Pyrolysis	413.0	503.0	10	100	< 250	228.60	
Tobacco Stem	40.89	7.09	39.95	Combustion	220.0	350.0	20	60	< 250	91.60	[38]
Sewage Sludge	40.40	6.20	45.70	Pyrolysis	240.0	330.0	5	200	1000	25.80	[39]
Sewage Sludge	40.40	6.20	45.70	Pyrolysis	240.0	330.0	10	200	1000	29.34	
Sewage Sludge	40.40	6.20	45.70	Pyrolysis	240.0	330.0	20	200	1000	27.40	
Sewage Sludge	40.40	6.20	45.70	Pyrolysis	400.0	550.0	5	200	1000	9.61	
Sewage Sludge	40.40	6.20	45.70	Pyrolysis	400.0	550.0	10	200	1000	1.31	
Sewage Sludge	40.40	6.20	45.70	Pyrolysis	400.0	550.0	20	200	1000	1.21	
Rice straw	47.93	6.25	43.58	Pyrolysis	217.0	341.0	10	100	150–180	55.76	[40]
Rice straw	47.93	6.25	43.58	Pyrolysis	255.0	389.0	20	100	150–180	58.06	
Rice straw	47.93	6.25	43.58	Pyrolysis	261.0	415.0	30	100	150–180	54.34	
Rice straw	47.93	6.25	43.58	Pyrolysis	289.0	473.0	40	100	150–180	63.88	
Pine sawdust	49.46	5.19	42.27	Pyrolysis	224.0	452.0	10	100	150–180	63.99	
Pine sawdust	49.46	5.19	42.27	Pyrolysis	249.0	464.0	20	100	150–180	53.28	
Pine sawdust	49.46	5.19	42.27	Pyrolysis	253.0	482.0	30	100	150–180	57.57	
Pine sawdust	49.46	5.19	42.27	Pyrolysis	268.0	493.0	40	100	150–180	60.14	
Phoenix tree leaves	51.84	5.39	39.69	Pyrolysis	225.0	426.0	10	100	150–180	32.29	
Phoenix tree leaves	51.84	5.39	39.69	Pyrolysis	233.0	444.0	20	100	150–180	49.29	
Phoenix tree leaves	51.84	5.39	39.69	Pyrolysis	241.0	467.0	30	100	150–180	83.64	
Phoenix tree leaves	51.84	5.39	39.69	Pyrolysis	248.0	500.0	40	100	150–180	178.57	
Acacia raw	47.08	5.77	47.04	Combustion	25.0	480.0	10	40	500	99.80	[41]
Acacia HTC	59.28	5.88	34.66	Combustion	25.0	520.0	10	40	500	95.80	
Pine raw	48.15	6.58	45.17	Combustion	25.0	500.0	10	40	500	89.30	
Pine HTC	62.83	6.50	30.61	Combustion	25.0	540.0	10	40	500	85.20	
SS raw	41.46	6.02	28.17	Combustion	25.0	495.0	10	40	500	44.30	
SS HTC	40.82	4.89	17.32	Combustion	25.0	470.0	10	40	500	37.40	
Hazelnut shell	46.30	5.80	47.50	Combustion	25.0	900.0	20	40	< 250	60.40	[42]
Lignite	53.20	5.50	36.00	Combustion	25.0	900.0	20	40	< 250	84.30	
2HS/98L	53.06	5.51	36.23	Combustion	25.0	900.0	20	40	< 250	68.90	
4HS/96L	52.92	5.51	36.46	Combustion	25.0	900.0	20	40	< 250	68.50	
6HS/94L	52.79	5.52	36.69	Combustion	25.0	900.0	20	40	< 250	67.60	
8HS/92L	52.65	5.52	36.92	Combustion	25.0	900.0	20	40	< 250	67.10	
10HS/90L	52.51	5.53	37.15	Combustion	25.0	900.0	20	40	< 250	66.80	
20HS/80L	51.82	5.56	38.30	Combustion	25.0	900.0	20	40	< 250	63.40	
MDF	49.57	6.33	39.66	Combustion	263.0	393.0	10	20	300–850	44.58	[43]
MDF	49.57	6.33	39.66	Combustion	270.0	400.0	20	20	300–850	47.67	
MDF	49.57	6.33	39.66	Combustion	285.0	413.0	30	20	300–850	50.02	
Particleboard	46.26	5.83	45.51	Combustion	260.0	360.0	10	20	300–850	53.67	
Particleboard	46.26	5.83	45.51	Combustion	260.0	360.0	20	20	300–850	55.73	
Particleboard	46.26	5.83	45.51	Combustion	270.0	400.0	30	20	300–850	59.10	
Plywood	47.12	5.92	45.72	Combustion	250.0	350.0	10	20	300–850	52.30	
Plywood	47.12	5.92	45.72	Combustion	250.0	370.0	20	20	300–850	61.27	
Plywood	47.12	5.92	45.72	Combustion	280.0	400.0	30	20	300–850	72.44	
Rice Husk	38.47	5.75	54.09	Pyrolysis	525.0	619.0	10	100	<250	59.23	[44]
Rice Husk	38.47	5.75	54.09	Pyrolysis	533.0	629.0	20	100	<250	58.19	
Rice Husk	38.47	5.75	54.09	Pyrolysis	538.0	641.0	30	100	<250	58.02	
Rice Husk	38.47	5.75	54.09	Pyrolysis	545.0	666.0	50	100	<250	65.16	
60AN40FV	84.11	4.50	7.91	Combustion	400.0	465.0	6	100	500–1000	134.31	[45]
60AN40FV	84.11	4.50	7.91	Combustion	410.0	489.0	12	100	500–1000	119.96	
60AN40FV	84.11	4.50	7.91	Combustion	425.0	526.0	24	100	500–1000	116.29	
60AN40FV	84.11	4.50	7.91	Combustion	465.0	556.0	6	100	500–1000	228.01	
60AN40FV	84.11	4.50	7.91	Combustion	489.0	580.0	12	100	500–1000	211.08	
60AN40FV	84.11	4.50	7.91	Combustion	526.0	636.0	24	100	500–1000	186.19	
NT	43.08	7.93	28.26	Pyrolysis	180.0	400.0	30	50	<425	17.09	[46]
NT	43.08	7.93	28.26	Pyrolysis	400.0	540.0	30	50	<425	8.04	
UT	43.54	8.17	28.04	Pyrolysis	180.0	400.0	30	50	<425	23.43	
UT	43.54	8.17	28.04	Pyrolysis	400.0	540.0	30	50	<425	9.19	
20AS/80IC	60.88	5.49	29.57	Combustion	190.0	353.0	10	45	<250	98.38	This
30AS/70IC	45.27	5.53	31.53	Combustion	180.0	355.0	10	45	<250	86.81	Study
40AS/60IC	57.09	5.57	33.49	Combustion	178.0	360.0	10	45	<250	87.11	
50AS/50IC	55.19	5.61	35.45	Combustion	170.0	360.0	10	45	<250	94.16	
60AS/40IC	53.30	5.64	37.41	Combustion	167.0	360.0	10	45	<250	89.92	
70AS/30IC	51.40	5.68	39.37	Combustion	160.0	360.0	10	45	<250	85.74	
80AS/20IC	49.51	5.72	41.34	Combustion	155.0	360.0	10	45	<250	82.85	
Almond	45.72	5.80	45.26	Combustion	150.0	365.0	10	45	<250	83.92	
20AS/80IC	60.88	5.49	29.57	Combustion	215.0	370.0	20	45	<250	106.30	

(*continued on next page*)

Table 3 (*continued*)

Sample	C (wt. %)	H (wt. %)	O (wt. %)	Thermolysis	TI (°C)	TF (°C)	HR (°C/min)	FR (ml/min)	Particle Size (μm)	Ea (kJ/mol)	Ref.
30AS/70IC	45.27	5.53	31.53	Combustion	200.0	375.0	20	45	<250	97.37	
40AS/60IC	57.09	5.57	33.49	Combustion	195.0	377.0	20	45	<250	98.60	
50AS/50IC	55.19	5.61	35.45	Combustion	190.0	375.0	20	45	<250	105.52	
60AS/40IC	53.30	5.64	37.41	Combustion	178.0	374.0	20	45	<250	96.77	
70AS/30IC	51.40	5.68	39.37	Combustion	172.0	380.0	20	45	<250	89.27	
80AS/20IC	49.51	5.72	41.34	Combustion	170.0	380.0	20	45	<250	93.17	
Almond	45.72	5.80	45.26	Combustion	160.0	380.0	20	45	<250	96.74	
20AS/80IC	60.88	5.49	29.57	Combustion	205.0	395.0	30	45	<250	93.89	
30AS/70IC	63.53	5.53	31.53	Combustion	195.0	395.0	30	45	<250	86.79	
40AS/60IC	57.09	5.57	33.49	Combustion	190.0	397.0	30	45	<250	87.31	
50AS/50IC	55.19	5.61	35.45	Combustion	188.0	398.0	30	45	<250	98.02	
60AS/40IC	53.30	5.64	37.41	Combustion	202.0	396.0	30	45	<250	95.49	
70AS/30IC	51.40	5.68	39.37	Combustion	185.0	400.0	30	45	<250	94.40	
80AS/20IC	49.51	5.72	41.34	Combustion	175.0	405.0	30	45	<250	91.77	
Almond	45.72	5.80	45.26	Combustion	170.0	405.0	30	45	<250	91.94	
Imbat	64.67	5.41	25.64	Combustion	225.0	650.0	10	45	<250	68.06	
20AS/80IC	60.88	5.49	29.57	Combustion	353.0	650.0	10	45	<250	70.56	
30AS/70IC	63.53	5.53	31.53	Combustion	355.0	635.0	10	45	<250	71.73	
40AS/60IC	57.09	5.57	33.49	Combustion	360.0	615.0	10	45	<250	76.75	
50AS/50IC	55.19	5.61	35.45	Combustion	360.0	610.0	10	45	<250	77.96	
60AS/40IC	53.30	5.64	37.41	Combustion	360.0	600.0	10	45	<250	80.41	
70AS/30IC	51.40	5.68	39.37	Combustion	360.0	585.0	10	45	<250	82.34	
80AS/20IC	49.51	5.72	41.34	Combustion	360.0	570.0	10	45	<250	86.87	
Almond	45.72	5.80	45.26	Combustion	365.0	515.0	10	45	<250	117.00	
Imbat	64.67	5.41	25.64	Combustion	240.0	850.0	20	45	<250	52.88	
20AS/80IC	60.88	5.49	29.57	Combustion	370.0	815.0	20	45	<250	47.16	
30AS/70IC	63.53	5.53	31.53	Combustion	375.0	770.0	20	45	<250	52.61	
40AS/60IC	57.09	5.57	33.49	Combustion	377.0	765.0	20	45	<250	52.82	
50AS/50IC	55.19	5.61	35.45	Combustion	375.0	735.0	20	45	<250	54.49	
60AS/40IC	53.30	5.64	37.41	Combustion	374.0	680.0	20	45	<250	64.44	
70AS/30IC	51.40	5.68	39.37	Combustion	380.0	680.0	20	45	<250	63.71	
80AS/20IC	49.51	5.72	41.34	Combustion	380.0	660.0	20	45	<250	67.79	
Almond	45.72	5.80	45.26	Combustion	380.0	600.0	20	45	<250	81.53	
Imbat	64.67	5.41	25.64	Combustion	260.0	970.0	30	45	<250	46.16	
20AS/80IC	60.88	5.49	29.57	Combustion	395.0	1020.0	30	45	<250	34.23	
30AS/70IC	63.53	5.53	31.53	Combustion	395.0	950.0	30	45	<250	37.85	
40AS/60IC	57.09	5.57	33.49	Combustion	397.0	875.0	30	45	<250	43.71	
50AS/50IC	55.19	5.61	35.45	Combustion	398.0	845.0	30	45	<250	47.23	
60AS/40IC	53.30	5.64	37.41	Combustion	396.0	798.0	30	45	<250	52.21	
70AS/30IC	51.40	5.68	39.37	Combustion	400.0	800.0	30	45	<250	64.33	
80AS/20IC	49.51	5.72	41.34	Combustion	405.0	800.0	30	45	<250	52.45	
Almond	45.72	5.80	45.26	Combustion	405.0	740.0	30	45	<250	62.64	

Experimental apparatus

TG experiments were conducted in a commercial "Netzsch 409 PC Luxx" contemporaneous thermogravimetric apparatus from NETZSCH-Feinmahltechnik GmbH, Germany. In the TGA tests, a sample mass of approximately 10.000 ± 1.000 mg was in Al_2O_3 crucible for each experiment. Oxygen (21 %) and argon (79 %) were used as a carrier gas with a flow rate of 45 ml/min for the entire co-combustion experiments. The experiments were carried out in non-isothermal conditions from ambient temperature to 1200 °C at heating rates of 10, 20, and, 30 °C/min.

Kinetic analysis

The primary reason for kinetic analysis is to discover the mechanisms of complex reactions that take place in the thermochemical conversion processes of solid fuels. Calculating Ea is essential to optimize the operating conditions and select a suitable reactor. Determination of the kinetic parameters such as Ea and pre-exponential factor (A) can be executed with TGA data. However, some assumptions including the selection of the reaction mechanism have to be made. Predominantly, the rate of conversion is stated for entire kinetic studies by the following basic rate equation [32]:

$$\frac{dx}{dt} = kf(x) \tag{1}$$

where "f(x)" stands for the reasonable-hypothetical model of the reaction mechanism, and various kinds of mechanisms have been reported in the literature [33], and "k" is the reaction rate constant. "x", which is conversion, can be described as follows:

$$x = \frac{w_i - w_t}{w_i - w_f} \tag{2}$$

where "w_t" indicates the weight of the sample at a specific time t (min), "w_i" mentions the initial weight and "w_f" refers to the final weight values of the sample (mg). By using the Arrhenius equation, the rate constant "k" can be calculated, whereby:

$$k = Ae^{\left(-\frac{Ea}{RT}\right)} \tag{3}$$

where "Ea" is the activation energy (kJ.mol^{-1}), "T" is the absolute temperature (K), "A" is the pre-exponential factor (min^{-1}) and "R" is the universal gas constant (8.314 J.(K^{-1}.mol^{-1})). The reaction rate can be expressed as follows by assembling Eqs. (1) and (3) [34]:

$$\frac{dx}{dt} = Ae^{\left(-\frac{Ea}{RT}\right)} f(x) \tag{4}$$

For dynamic TGA operation (non-isothermal), β = dT/dt, to substitute the heating rate β, expression becomes:

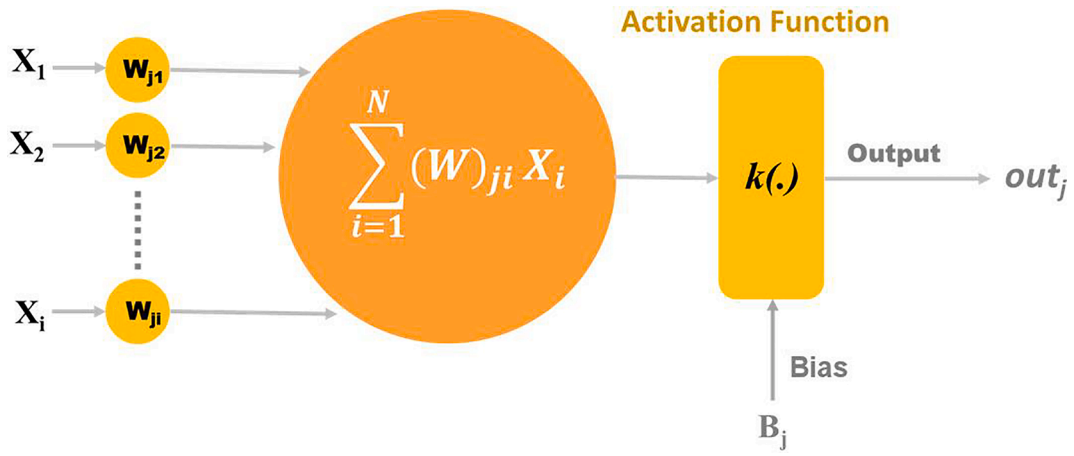

Fig. 1. The schematic representation of the artificial node.

$$\frac{dx}{dT} = \left(\frac{A}{\beta}\right) e^{\left(-\frac{Ea}{RT}\right)} f(x) \tag{5}$$

The integral form of Eq. (5) can be depicted as:

$$g(x) = \int_0^x \frac{dx}{f(x)} = \frac{A}{\beta} \int_{T0}^{T} e^{\left(-\frac{Ea}{RT}\right)} dT \tag{6}$$

where "g(x)" is an integral form of reaction model. Since an analytical solution of the right side of the equation is impossible, various approaches have been offered for the solution. One of the most popular models is the Coats-Redfern [35]. Basic form of the Coats-Redfern model is given as follows:

$$ln\frac{g(x)}{T^2} = ln\left[\frac{AR}{\beta Ea}\left(1 - \frac{2RT}{Ea}\right)\right] - \frac{Ea}{RT} \tag{7}$$

Plotting the left-hand side of Eqn. (7), which includes g(x) versus 1/T, gives Ea and A from the slope and intercept respectively. Generally, the model that provides the most precise fitting is selected as the correct model. In this study, Ea values were calculated using the Coats-Redfern method with the first order chemical reaction where f(x) = 1-x and g(x) = −ln(1-x).

Data collection

In this study, TGA experiments in the literature were reviewed in order not to be dependent on our experimental work. In addition to the experimental findings of the combustion process in an air environment, the results of the pyrolysis process in an inert environment acquired through the literature study are included. Although some of the kinetic results were reported for both TGA and different types of reactors, only kinetic data derived from TGA were included in the dataset. Table 3 summarizes the ultimate analysis properties of the fuels including biomass, municipal wastes/sludges, polymers, lignites, and various blends and the experimental TGA results of these fuels used for the developed model in this study.

E.rigida represents Euphorbia rigida, PET represents polyethylene terephthalate, PVC represents polyvinyl chloride, CS represents cotton stalk, HS represents hazelnut shell, SFR represents sunflower residue, ER represents E.rigida, HS/L represents hazelnut shell/lignite blend, MDF represents medium density fiber, HTC represents hydrothermal carbonization, AN/FV represents anthracite/Ficus virens blend, UT and NT represent ultrasonic treatment and no treatment on waste activated sludge respectively, and AS/IC represents almond shell/İmbat coal blend. As can be seen in Table 3, the TGA experiments were conducted under inert and oxidative (air) atmospheres. Solid fuels consist of biomass, coal and blends of these in different proportions. There are also differences in the experimental conditions such as heating rate (HR), flow rate in purge (FR), particle size, initial and final temperatures of the different stages. However, all Ea values obtained from the literature were calculated using the Coats-Redfern method for a first order chemical reaction model.

Artificial neural network

ANNs are machine learning approaches that use computational tools [47]. They are excellent alternative input/output mapping learners [48]. Their fundamental structure is based on neurons in the human nervous system [49] and called artificial neuron or artificial node (perceptron). The artificial nodes are established by using the weight function and the activation function. The structure of a perceptron is shown in Fig. 1.

ANNs are extremely strong predictors; it has been mathematically demonstrated that given sufficient training process and data, an ANN can acquire any mathematical function with adequate accuracy [50]. Besides, black-box models are the functional connections between system inputs and outputs. In terms of equivalence to process factors such as heat or mass transfer coefficients, reaction kinetics, and so on, the parameters of these equations have no physical meaning [51]. An ANN is a black-box in the notion that, while it can estimate any function, understanding its structure will reveal nothing about the nature of the function it is attempting to approximate. An artificial neuron is activating the weighted sum of inputs from the previous layer of nodes (Fig. 1) including the bias value. The formula of a perceptron can be expressed as:

$$Y = \left(\sum_{i=1}^{n} X_i . W_{ji} + B_j\right) \tag{8}$$

where "X_i" represents the input from the previous layer's "i_{th}" artificial neuron, and each "X_i" has a weight "W_{ji}" that indicates the strength of the link between the "j_{th}" artificial neuron and the current artificial neuron. The perceptron adds the "X_i" and "W_{ji}" to get a weighted summation, which it feeds into the activation function "k" together with a bias "B_j". Finally, the output of an artificial node j is given by:

$$out_j = k(Y) \tag{9}$$

It is vital to choose an appropriate activation function in order to alter all of the weights in order to minimize the difference between the predicted output and the actual output. The activation function can be found in various forms, either linear or nonlinear. The linear function is determined for the output layer. Further, the "tangent sigmoid (tansig)"

Table 4
A statistical description of the dataset.

	Range	Mean	Std
C (wt %, daf)	38.47–84.11	54.24	8.97
H (wt %, daf)	3.90–8.17	5.61	0.63
O (wt %, daf)	7.91–54.09	38.24	8.79
TI (°C)	25.00–562.00	247.35	132.83
TF (°C)	77.00–1020.00	450.91	201.57
HR (°C/min)	5.00–50.00	16.62	9.56
FR (ml/min)	20.00–200.00	76.57	37.48
Ea (kJ/mol)	1.21–347.40	85.95	54.91

function is frequently used in the hidden layer as a nonlinear activation function for predictions. In this study, "tansig" function was used as an activation function which can be expressed as:

$$f(x) = \frac{e^{x} - e^{-x}}{e^{x} + e^{-x}} \tag{10}$$

Training & optimization of ANN model

In general, the architecture (number of layers), the topology (connective pattern, feed-forward or recurrent, etc.) and the learning regime are the main considerations for the neural network categorization [52]. Among the proposed ANN models, the Multilayer Perceptron (MLP), which is a layered feed-forward neural network, is often preferred structure. Typically, the MLP structure includes an input layer, one or more hidden layers, and an output layer with associated perceptron on the output layer. During the design of the neural network structure, the hidden layer and the number of artificial neurons (perceptrons) are determined by reducing the error of the network using a trial-and-error approach [53]. The bias and weight values of the network layers are rearranged to minimize the error by iteratively backpropagating the error values using a learning algorithm, which is the backpropagation algorithm in this study. However, the optimization technique to be employed, the number of layers, and the number of neurons in each layer are all selected using this approach by doing trials until the MSE converges to the lowest value. Thus, the sequential model's performance has been enhanced, and the model is able to make accurate predictions for new instances. On the other hand, excessive epochs for training can lead to an overfit, while too few epochs for training can lead to an underfit. The validation dataset is used to specify an arbitrary number of

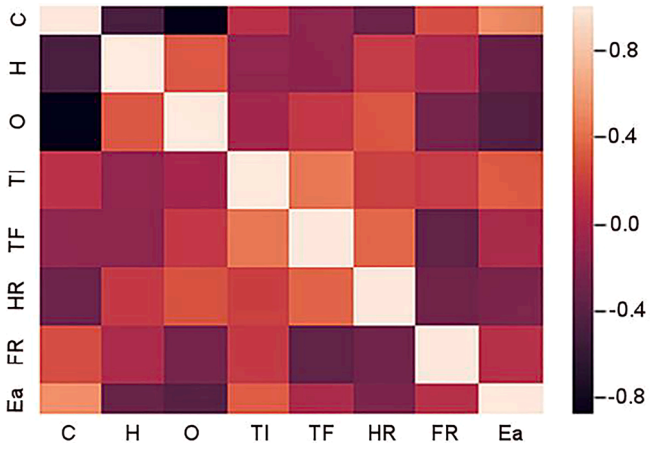

Fig. 3. The correlation map.

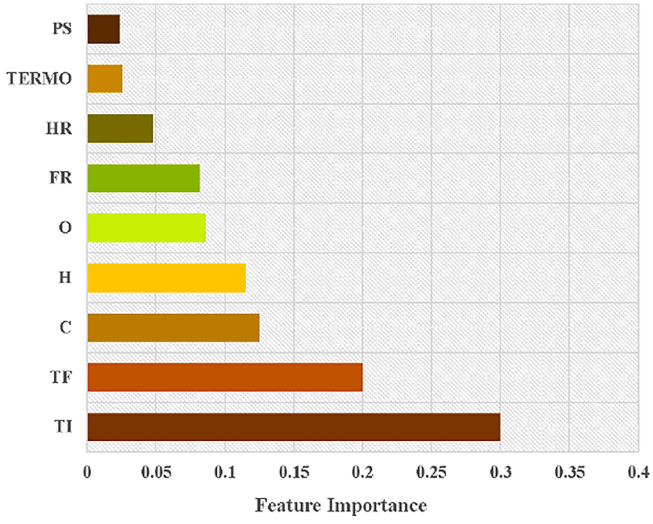

Fig. 4. Feature importance for Ea prediction.

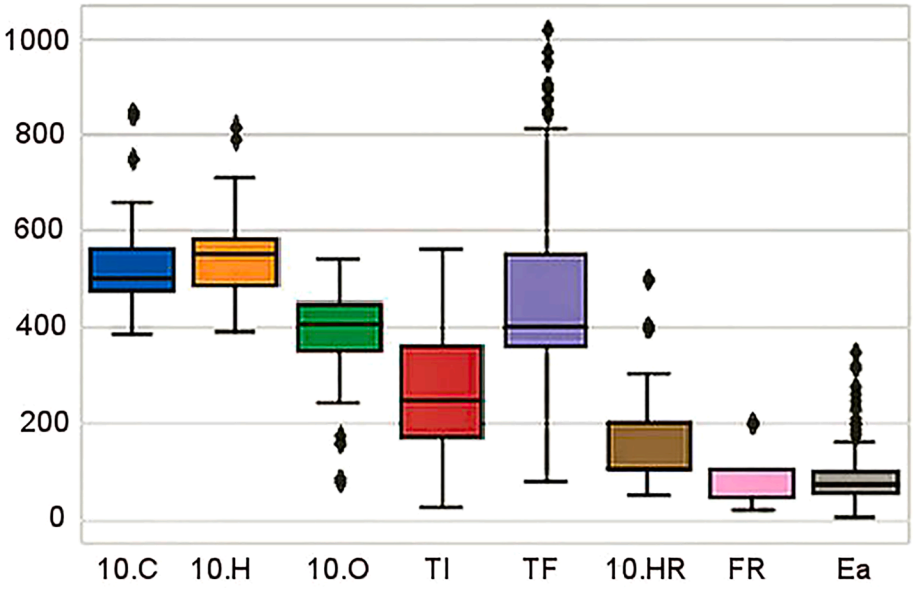

Fig. 2. Variation of individual input values in the data set.

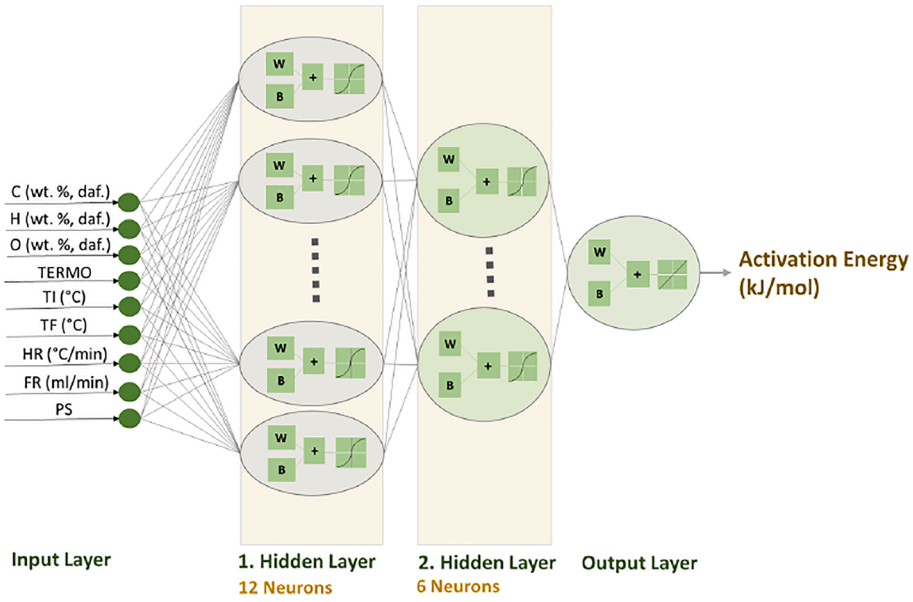

Fig. 5. The ANN structure used for the prediction of Ea.

Table 5
The learning and training parameters.

Learning parameter	Value
Optimizer	Levenberg-Marquardt
Loss Function	Mean absolute percentage error
Training parameter	**Value**
Training split	0.80
Validation split	0.05
Test split	0.15
Epochs	1000

epochs and stop training when the model's performance on a holdout loss function for validation dataset reaches a certain point [54]. The test dataset is not used for training to ensure that the performance of the model is evaluated independently of the training dataset. The model topology in this study was developed by using the "MATLAB® (R2019a)" software via "Neural Networks Toolbox" library.

Error evaluation

The criteria considered in calculating the difference between the actual values and the predicted values for the training dataset and the test dataset for the selected artificial neural network structure in this study are the mean absolute percentage error (MAPE) in Eq. (11) and the coefficient of determination (R^2) in Eq. (12):

Table 6
MAPE results for the training and the test.

	Activation Energy Prediction
MAPE (Training)	12.22 %
MAPE (Test)	19.66 %

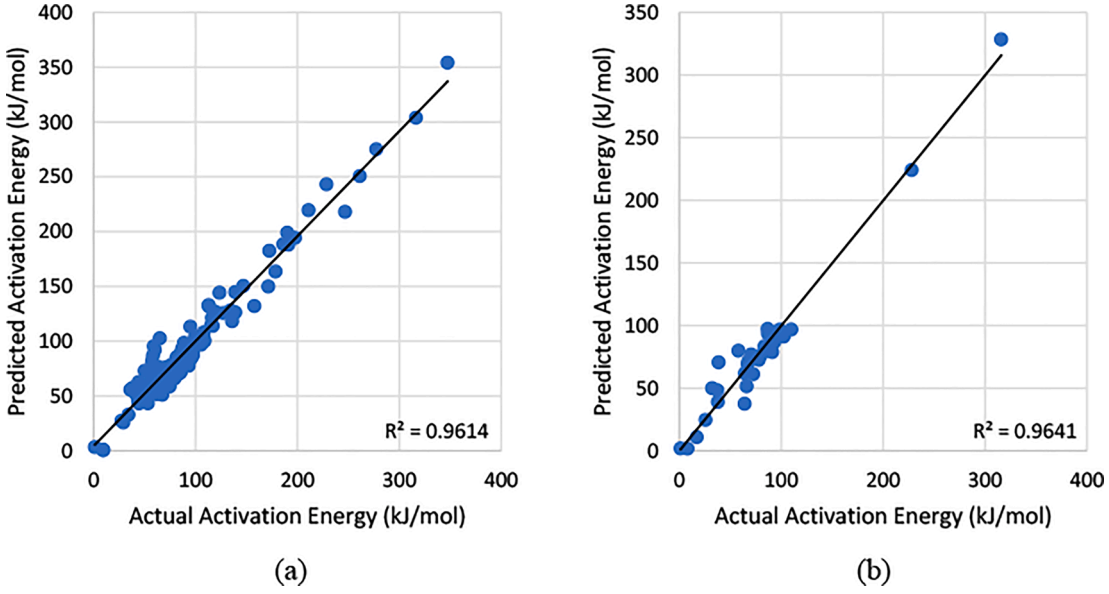

Fig. 6. Comparison of R^2 values for the Ea values for the (a) training and (b) test.

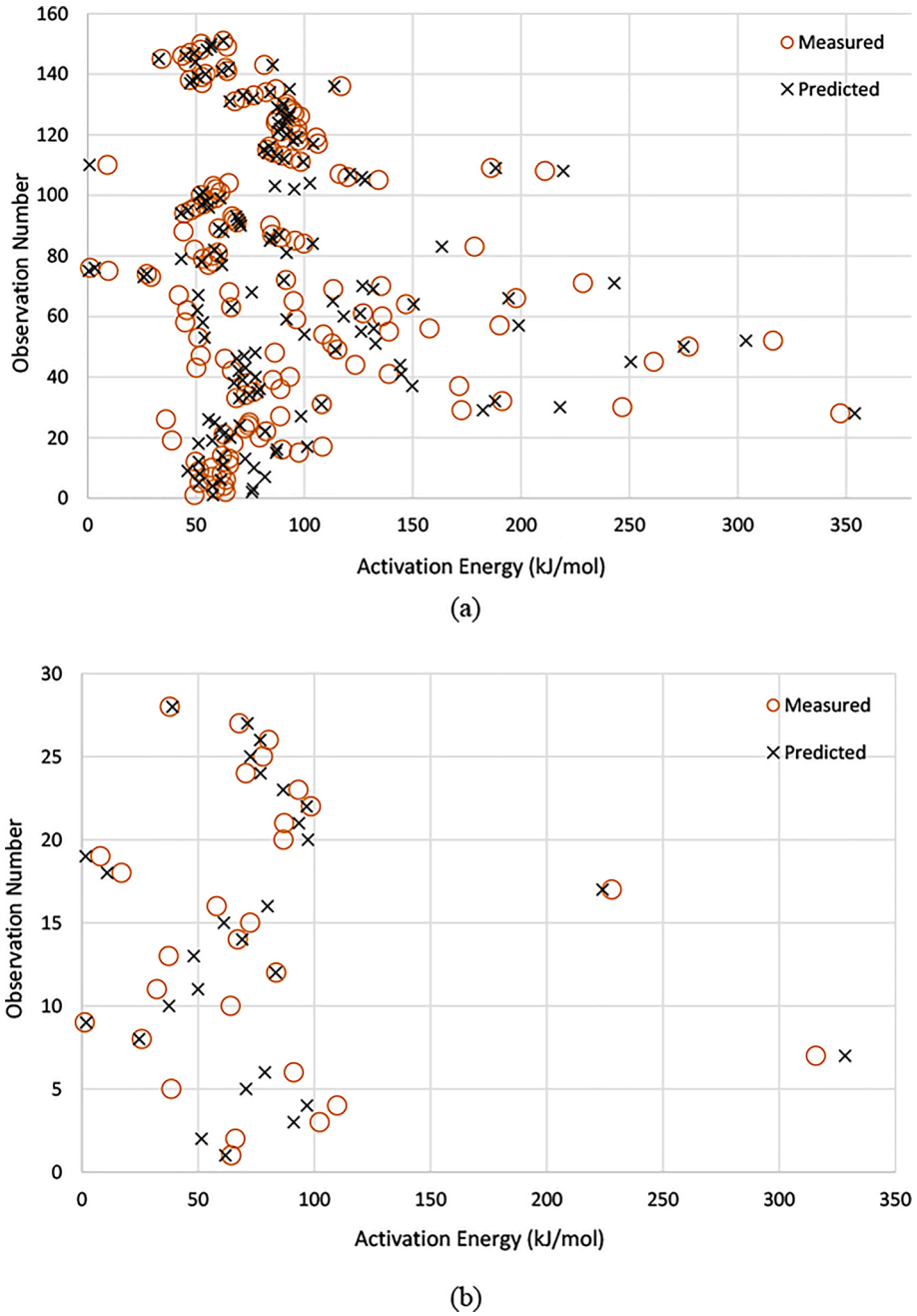

Fig. 7. The calculated and forecasted Ea values: (a) Training, (b) Test.

$$MAPE = \frac{100}{n}\sum_{i=1}^{n}\left|\frac{Y_{iactual} - Y_{ipredicted}}{Y_{iactual}}\right| \quad (11)$$

$$R^2 = 1 - \frac{\sum_{i=1}^{n}(Y_{ipredicted} - Y_{iactual})^2}{\sum_{i=1}^{n}(Y_{ipredicted} - Y_{mean})^2} \quad (12)$$

where "n", "$Y_{ipredicted}$", "$Y_{iactual}$" and "Y_{mean}" are the number of instances, the produced value by the ANN model and the target value for the i_{th} instance, and the mean value of target outputs, respectively.

Results

Dataset preparation and statistical analysis

The dataset created in this subsection is statistically analyzed, as well as the information about the input/output parameters to which the ANN fits. Furthermore, the relationships between the input/output parameters and the compatibility with the scientific background are examined. Finally, by assessing the relative importance of the input variables, the most significant features were identified, and information is provided for the input variables to be selected/developed in future studies. Each input set includes the elemental composition (wt%, daf.) of the solid fuel, the atmospheric flow rate, the heating rate, and the initial and final decomposition stage temperatures. The ultimate analysis results for the feedstocks are on a dry ash-free basis (wt%), and the essential conversions were made for results published on a different basis. The parameters used as input variables in this study are as follows:

- C: Elemental carbon content (wt%, daf.) in the solid material.
- H: Elemental hydrogen content (wt%, daf.) in the solid material.

- O: Elemental oxygen content (wt%, daf.) in the solid material.
- TI: The temperature (°C) at which thermal decomposition begins.
- TF: The temperature (°C) at which thermal decomposition ends.
- HR: The heating rate (°C/min) of the furnace specified for the thermochemical procedure.
- FR: The flow rate of operational gas (ml/min) specified for the thermochemical procedure.
- Ea: The activation energy (kJ/mol) obtained as a result of the kinetic analysis procedure.
- TERMO: The type of thermochemical process that taking place in TGA.
- PS: The particle size class of the solid material used in TGA.

TERMO and PS are assigned as boolean values. When the TGA is performed in the air atmosphere in which the combustion experiments take place, TERMO is equal to 1, and when it is performed under an inert atmosphere in which the pyrolysis experiments take place, TERMO is equal to 0. Moreover, using a similar approach for PS, a value$<$250 μm was assigned as 0 and a greater value as 1. The reason why 250 μm was set as the threshold value is that the particle size larger than 200 μm affects the fast pyrolysis of biomass [55]. Table 4 briefly describes the dataset.

The table demonstrates that the Ea is in a wide range, and the standard deviation is high. Although the HR varies depending on the capacity of the device, it is approximately at certain values (5, 10, 20, 30, 40, 50 °C.min^{-1}) in TGA experiments. Further, the FR was frequently determined as 100 ml/min in the literature, but since the FR was selected as 45 ml/min in this study, the mean value was decreased. The boxplot of the features and the targets are shown in Fig. 2.

It is observed in Fig. 2 that TI and TF values are in a wide scale. The number of pseudo components is decided by examining the change of TG curves. For biomass and coal, the number of pseudo components is usually-two (volatile matters and carbon content). However, some authors have calculated single Ea by assuming the solid fuel as a single pseudo component. Therefore, the initial and final temperatures of the degradation stages vary depending on the physicochemical properties of the solid fuel, as well as the number of pseudo components. Moreover, many possible outliers were seen for the final temperature value. The presence of many possible outliers for Ea also makes it a complex parameter to predict.

After examining the relationships between the parameters, it can be concluded that an advanced learning network should be constructed for Ea prediction. The relationships between features and target are shown in Fig. 3.

In Fig. 3, it can be seen that the correlation coefficients are mostly between the values + 0.4 and −0.4. Therefore, there may be no evidence of a strong linear relationship between features and targets. However, the lack of a strong linear association between values does not always imply the absence of any other type of association between the two variables.

There are negative correlations between C—O and C—H for numerical reasons, and this is because the ultimate analysis result on a dry ash-free basis should total close to 100. Similarly, when the TI increases the TF increases as well because the decomposition process that was started at high temperatures was ended at higher temperatures. Further, the high HR reduced the Ea value, according to the correlation map. Exposure of the solid fuel to high heat per unit time has constituted the cracking process to occur easier. This phenomenon has also been observed by other authors [45]. However, there is not any certain rule that the HR increases [56] or decreases [57] the Ea value because the properties of the fuel and the kinetic analysis methods are also absolutely crucial.

It is thoroughly experienced that the Ea is highly related to the reactivity and structure of the material. The devolatilization of VM content takes place at lower temperatures in the first zone. Further in the first stage, molecules are slow and the Ea value is higher for reactivity [58], thus the Ea value in the volatile oxidation zones are often higher than those in the FC combustion step, which is in agreement with the literature [59–60]. Conversely, the required Ea for the first stage in the pyrolytic atmosphere is lower than the required Ea for the second stage. Contrary to the combustion process, the pyrolysis process is endothermic and requires more energy to crack the heavier organic structures in the solid fuel, resulting in higher Ea in the second stage. This occurrence has also been observed by other researchers [15]. However, it is not a reliable method to analyze the change of a single parameter and interpret its effect on Ea. The researchers conducted TGA experiments under different operating conditions using several fuels with various physicochemical properties. Furthermore, there are differences in determining the initial and final temperatures while dividing the degradation process into different zones. In conclusion, it is problematic to assemble a linear relationship between input variables and the Ea. Additionally, the feature importance method [61] was used to examine the relative contributions of the model properties in the estimation of Ea. Fig. 4 visualizes the feature importance.

Expectedly, temperature is the most important parameter that affects the Ea value. Approximately, TI and TF constitute 50 % of the importance ranking. The behavior of the TG curve changes in a non-isothermal heating program depending on the conversion, and thus the temperature. Therefore, various complex reactions take place depending on the temperature during thermal decomposition. Inevitably, diverse degradation characteristics lead to the calculation of different Ea values. Apart from the TI and TF properties, the most effective model properties are C, H and O, contributing about 30 %. Although the elemental composition of biomass and coal largely includes these three elements, the amount of each individual varies considerably. Further, biomass and coal contain different chemical structures, bonds and physicochemical properties which are highly influential on thermal degradation profile. Considering all these facts, it is unrealistic to calculate the same Ea value for different fuels in the identical temperature interval. Operating conditions seem to be the least effective among all model features. However, these parameters are quite critical not to be neglected and should be included as model features for a realistic TGA simulation. In thermolysis processes, Ea changes depending on the HR [62], and FR may affect the possibility of solid–gas reactions. In addition, PS is one of the primary parameters affecting the thermolysis behavior of solid fuels and has a dominant effect on mass and heat transfer mechanisms, weight loss and Ea values [22]. On the other hand, the effect of particle size on the selected reaction should be very small compared to the initial temperature, and we can observe this comparison in Fig. 4.

Assessment of the ANN model

To improve the model's generalization performance, the produced dataset is randomly divided into three datasets: 80 % for training (151 datasets), 15 % for testing (28datasets), and 5 % for validation (9datasets). After the trial-and-error procedure, the most suitable network topology for multilayer perceptron model was determined. Fig. 5 shows the overall structure of the ANN model created in this study.

The input layer contains nine parameters: O, H, C, TERMO, TI, TF, HR, FR and PS. The output value generated by the first hidden layer is processed as the input value of the second hidden layer with 6 neurons after the model input values have been processed in the first hidden layer with 12 neurons. The tansig activation function, which gives good results in engineering problems, is used in both hidden layers. The activation function is used to send the data processed in the hidden layers to the output layer to calculate the Ea value. The optimizer decides how to update the network weights based on the output of the loss function. In this study, the Levenberg-Marquardt optimizer was preferred for the evaluation. Table 5 lists the learning and training parameters of the ANN model.

The correlation coefficient R^2 is generally-one of the most commonly used parameters to evaluate the relationship between the target value and the predicted value as the performance of a model. Fig. 6 shows a comparison of the correlation coefficient values for the Ea predictions.

The R^2 values are greater than 0.96 for both training and testing, as shown in Fig. 6. The ANN model is able to reliably estimate the Ea values for the TGA experiments. Although the physicochemical properties of the solid fuels in the data set vary and the operating conditions are different, the ANN model successfully predicts the Ea value. Beyond that, the MAPE results for target values are summarized in Table 6.

Table 6 denotes that the MAPE values for the training set and the test set are acceptably low. These results imply that the ANN model shows a satisfactory performance. An image of the calculated and estimated Ea values is presented in Fig. 7.

It is observed from the plots that Ea values are densely located between 50 and 150 kJ/mol. Nevertheless, output variable includes some extreme values up to 350 kJ/mol. Despite this wide range of output values, the newly developed ANN model made successful predictions for both testing and training. In testing, no common characteristics were detected among the eight perfectly fitted samples (cross and circle overlap). The Ea values ranged from 1.31 kJ/mol to 228.01 kJ/mol, and the samples were representative of both the pyrolysis and combustion processes, with a diversity of physicochemical features. These samples are 70AS/30IC (sample 1), sewage sludge (sample 8), sewage sludge (sample 9), phoenix tree leaves (sample 12), plywood (sample 14), 60AN/40FV (sample 17), 40AS/60IC (sample 22) and 30AS/70IC (sample 28). As a consequence, it is worth mentioning that the ANN model is not specialized to any certain fuel type or operating conditions. Unlike the studies reported in the literature, a realistic simulation of the TG analyzer was performed with the ANN model where the effect of various input values was evaluated, and different type of fuels were included.

Conclusions

The utilization of solid fuels in primary energy sources as well as chemical conversion with a variety of cycles requires the study of their kinetics. Therefore, TGA is one of the most widely used techniques for kinetic characterization of solid fuels. In this study, a practical simulation of a thermogravimetric analyzer was performed for kinetic calculation. Unlike similar studies in the literature, fuel particle size, operating parameters for thermogravimetric analyzer were chosen as input parameters. The shortcoming of this study is that the combination of fuel type and operating conditions involves an infinite number of possibilities, and it is impossible to obtain so many experimental results. For this reason, elemental analysis values were also used in this study to define solid fuels. This allowed us to define an infinite number of different types of fuels as input parameters to the model. Thus, the model allows us to calculate the kinetic parameters for the pyrolysis and combustion reactions of fuels that were not considered in this study. Results showed that the newly developed ANN model can predict the activation energy as a kinetic calculation with an acceptable margin of error. The R^2 score is greater than 0.96, and the MAPE value is <20 %, according to the results. Moreover, with approximately 50 % score, the initial and final temperatures of the thermal decomposition process are the most important parameters in the prediction of Ea. This outcome is quite consistent with the theoretical background, given that various structures in solid fuel degrade at different temperatures.

Declaration of Competing Interest

The authors declare that they have no known competing financial interests or personal relationships that could have appeared to influence the work reported in this paper.

References

[1] M. Inayat, S.A. Sulaiman, J.C. Kurnia, M. Shahbaz, Effect of various blended fuels on syngas quality and performance in catalytic co-gasification: A review, Renew. Sust. Energ Rev. 105 (2019) 252–267.

[2] E. Abokyi, P. Appiah-Konadu, F. Abokyi, E.F. Oteng-Abayie, Industrial growth and emissions of CO2 in Ghana: The role of financial development and fossil fuel consumption, Energy Rep. 5 (2019) 1339–1353.

[3] J.A. Okolie, S. Nanda, A.K. Dalai, F. Berruti, J.A. Kozinski, A review on subcritical and supercritical water gasification of biogenic, polymeric and petroleum wastes to hydrogen-rich synthesis gas, Renew. Sust. Energ Rev. 119 (2020) 109546.

[4] Statistics I, Key world energy statistics, Paris, France, International Energy Agency, 2014.

[5] S. Wang, G. Dai, H. Yang, Z. Luo, Lignocellulosic biomass pyrolysis mechanism: a state-of-the-art review, Prog. Energ. Combust. Sci. 62 (2017) 33–86.

[6] Q.-V. Bach, Ø. Skreiberg, Upgrading biomass fuels via wet torrefaction: A review and comparison with dry torrefaction, Renew. Sust. Energ Rev. 54 (2016) 665–677.

[7] A. Sarvaramini, G.P. Assima, G. Beaudoin, F. Larachi, Biomass torrefaction and CO2 capture using mining wastes–A new approach for reducing greenhouse gas emissions of co-firing plants, Fuel 115 (2014) 749–757.

[8] P. Manara, A. Zabaniotou, Towards sewage sludge based biofuels via thermochemical conversion–A review, Renew. Sust. Energ Rev. 16 (5) (2012) 2566–2582.

[9] Ö. Çepelioğullar, İ. Mutlu, S. Yaman, H. Haykiri-Acma, Activation energy prediction of biomass wastes based on different neural network topologies, Fuel 220 (2018) 535–545.

[10] U. Özveren, Theoretical and Experimental Investigation Of Biomass And Coal Gasification, Marmara University, Istanbul, 2013.

[11] M. Müller-Hagedorn, H. Bockhorn, L. Krebs, U. Müller, A comparative kinetic study on the pyrolysis of three different wood species, J. Anal. Appl. Pyrol. 68 (2003) 231–249.

[12] S. Szymkuć, E.P. Gajewska, T. Klucznik, K. Molga, P. Dittwald, M. Startek, M. Bajczyk, B.A. Grzybowski, Computer-assisted synthetic planning: The end of the beginning, Angew. Chem. Int. Ed. 55 (20) (2016) 5904–5937.

[13] T. Lu, C.K. Law, Toward accommodating realistic fuel chemistry in large-scale computations, Prog Energ Combust Sci. 35 (2) (2009) 192–215.

[14] B. Ye, R. Zhang, J. Cao, K. Lei, D. Liu, The study of co-combustion characteristics of coal and microalgae by single particle combustion and TGA methods, J. Energy Inst. 93 (2) (2020) 508–517.

[15] Ö. Çepelioğullar, A.E. Pütün, Thermal and kinetic behaviors of biomass and plastic wastes in co-pyrolysis, Energ Conv Manag. 75 (2013) 263–270.

[16] M. Ashraf, Z. Aslam, N. Ramzan, U. Aslam, A.K. Durrani, R.U. Khan, et al., Pyrolysis of cattle dung: model fitting and artificial neural network validation approach, Biomass Convers. Biorefin. (2021) 1–12.

[17] A. Farooq, M. Ashraf, Z. Aslam, A. Anwar, S. Jiang, A. Farooq, et al., Pyrolytic conversion of a novel biomass Ficus natalensis barkcloth: physiochemical and thermo-kinetic analysis, Biomass Convers. Biorefin. (2021) 1–15.

[18] M. Ashraf, N. Ramzan, R.U. Khan, A.K. Durrani, Analysis of mixed cattle manure: kinetics and thermodynamic comparison of pyrolysis and combustion processes, Case Studies in Thermal Engineering. 26 (2021) 101078.

[19] R. Barzegar, A. Yozgatligil, H. Olgun, A.T. Atimtay, TGA and kinetic study of different torrefaction conditions of wood biomass under air and oxy-fuel combustion atmospheres, J. Energy Inst. 93 (3) (2020) 889–898.

[20] Z.R. Gajera, K. Verma, S.P. Tekade, A.N. Sawarkar, Kinetics of co-gasification of rice husk biomass and high sulphur petroleum coke with oxygen as gasifying medium via TGA, Bioresour. Technol. Rep. 11 (2020) 100479.

[21] Z. Wu, S. Wang, J. Zhao, L. Chen, H. Meng, Synergistic effect on thermal behavior during co-pyrolysis of lignocellulosic biomass model components blend with bituminous coal, Bioresour. Technol. 169 (2014) 220–228.

[22] K.K. Dwivedi, Prabhansu, M.K. Karmakar, P.K. Chatterjee, Thermal degradation, characterization and kinetic modeling of different particle size coal through TGA, Thermal Sci. Eng. Progress. 18 (2020) 100523.

[23] S. Mullainathan, J. Spiess, Machine learning: an applied econometric approach, J. Econ. Perspect. 31 (2) (2017) 87–106.

[24] Shokri R, Stronati M, Song C, Shmatikov V, editors. Membership inference attacks against machine learning models. 2017 IEEE Symposium on Security and Privacy (SP); 2017: IEEE.

[25] M. Haenlein, A. Kaplan, A brief history of artificial intelligence: On the past, present, and future of artificial intelligence, California Manage. Rev. 61 (4) (2019) 5–14.

[26] S.K. Arumugasamy, A. Selvarajoo, Feedforward neural network modeling of biomass pyrolysis process for biochar production, Chem. Eng. Trans. 45 (2015) 1681–1686.

[27] R. Mikulandrić, D. Lončar, D. Böhning, R. Böhme, M. Beckmann, Artificial neural network modelling approach for a biomass gasification process in fixed bed gasifiers, Energ Conv Manag. 87 (2014) 1210–1223.

[28] Pitel J, Mizak J, editors. Approximation of CO/lambda biomass combustion dependence by artificial intelligence techniques. Annals of DAAAM for 2011 & Proceedings of the 22nd International DAAAM Symposium; 2011: DAAAM International.

[29] S. Sunphorka, B. Chalermsinsuwan, P. Piumsomboon, Application of artificial neural network for kinetic parameters prediction of biomass oxidation from biomass properties, J. Energy Inst. 90 (1) (2017) 51–61.

[30] W. Jiang, X. Xing, X. Zhang, M. Mi, Prediction of combustion activation energy of NaOH/KOH catalyzed straw pyrolytic carbon based on machine learning, Renew Energ. 130 (2019) 1216–1225.

[31] D. Van Krevelen, Graphical-statistical method for the study of structure and reaction processes of coal, Fuel 29 (1950) 269–284.
[32] S. Vyazovkin, A.K. Burnham, L. Favergeon, N. Koga, E. Moukhina, L.A. Pérez-Maqueda, N. Sbirrazzuoli, ICTAC Kinetics Committee recommendations for analysis of multi-step kinetics, Thermochim. Acta 689 (2020) 178597.
[33] N. Liu, W. Fan, R. Dobashi, L. Huang, Kinetic modeling of thermal decomposition of natural cellulosic materials in air atmosphere, J. Anal. Appl. Pyrol. 63 (2) (2002) 303–325.
[34] Q.-V. Bach, W.-H. Chen, Pyrolysis characteristics and kinetics of microalgae via thermogravimetric analysis (TGA): a state-of-the-art review, Bioresour. Technol. 246 (2017) 88–100.
[35] A.W. Coats, J. Redfern, Kinetic parameters from thermogravimetric data, Nature 201 (4914) (1964) 68–69.
[36] Y. Zhang, Y. Niu, H. Zou, Y.u. Lei, J. Zheng, H. Zhuang, S. Hui, Characteristics of biomass fast pyrolysis in a wire-mesh reactor, Fuel 200 (2017) 225–235.
[37] B.B. Uzun, E. Yaman, Pyrolysis kinetics of walnut shell and waste polyolefins using thermogravimetric analysis, J. Energy Inst. 90 (6) (2017) 825–837.
[38] Z. Yang, S. Zhang, L. Liu, X. Li, H. Chen, H. Yang, X. Wang, Combustion behaviours of tobacco stem in a thermogravimetric analyser and a pilot-scale fluidized bed reactor, Bioresour. Technol. 110 (2012) 595–602.
[39] S.R. Naqvi, R. Tariq, Z. Hameed, I. Ali, M. Naqvi, W.-H. Chen, S. Ceylan, H. Rashid, J. Ahmad, S.A. Taqvi, M. Shahbaz, Pyrolysis of high ash sewage sludge: Kinetics and thermodynamic analysis using Coats-Redfern method, Renew Energ. 131 (2019) 854–860.
[40] R. Xiao, W. Yang, X. Cong, K. Dong, J. Xu, D. Wang, X. Yang, Thermogravimetric analysis and reaction kinetics of lignocellulosic biomass pyrolysis, Energy. 201 (2020) 117537.
[41] M. Wilk, A. Magdziarz, K. Jayaraman, M. Szymańska-Chargot, I. Gökalp, Hydrothermal carbonization characteristics of sewage sludge and lignocellulosic biomass, A comparative study. Bio and Bioenerg. 120 (2019) 166–175.
[42] H. Haykiri-Acma, S. Yaman, Effect of co-combustion on the burnout of lignite/biomass blends: a Turkish case study, Waste Manage. 28 (11) (2008) 2077–2084.
[43] S.Y. Yorulmaz, A.T. Atimtay, Investigation of combustion kinetics of treated and untreated waste wood samples with thermogravimetric analysis, Fuel Process. Technol. 90 (7–8) (2009) 939–946.
[44] A.C. Minh Loy, S. Yusup, B.L. Fui Chin, D.K. Wai Gan, M. Shahbaz, M.N. Acda, P. Unrean, E. Rianawati, Comparative study of in-situ catalytic pyrolysis of rice husk for syngas production: kinetics modelling and product gas analysis, J. Cleaner Prod. 197 (2018) 1231–1243.
[45] W. Tong, Q. Liu, G. Ran, L. Liu, S. Ren, L. Chen, L. Jiang, Experiment and expectation: Co-combustion behavior of anthracite and biomass char, Bioresour. Technol. 280 (2019) 412–420.
[46] H. Jia, B. Liu, X. Zhang, J. Chen, W. Ren, Effects of ultrasonic treatment on the pyrolysis characteristics and kinetics of waste activated sludge, Environ. Res. 183 (2020) 109250.
[47] T.M. Mitchell, Does machine learning really work? AI magazine. (1997;18(3):11-.).
[48] J.S. Hallinan, Computational intelligence in the design of synthetic microbial genetic systems, Methods in Microbiology. 40 (2013) 1–37.
[49] M.J. Diamantopoulou, E. Milios, D. Doganos, I. Bistinas, Artificial Neural Network Modeling for Reforestation Design through the Dominant Trees Bole-Volume Estimation, Nat. Resour. Model. 22 (4) (2009) 511–543.
[50] R. Hecht-Nielsen, Theory of the backpropagation neural network, Elsevier, Neural networks for perception, 1992, pp. 65–93.
[51] P. Zhang, Advanced industrial control technology, William Andrew (2010).
[52] S. Mesroghli, E. Jorjani, S. Chelgani, Estimation of gross calorific value based on coal analysis using regression and artificial neural networks, Int. J. Coal Geol. 79 (1–2) (2009) 49–54.
[53] D.-C. Lo, C.-C. Wei, E.-P. Tsai, Parameter automatic calibration approach for neural-network-based cyclonic precipitation forecast models, Water. 7 (7) (2015) 3963–3977.
[54] J.M. Ortíz Rodríguez, M.R. Martínez Blanco, J.M. Cervantes Miramontes, H. R. Vega Carrillo, Robust design of artificial neural networks methodology in neutron spectrometry, IntechOpen (2013).
[55] M. Van de Velden, J. Baeyens, A. Brems, B. Janssens, R. Dewil, Fundamentals, kinetics and endothermicity of the biomass pyrolysis reaction, Renew Energ. 35 (1) (2010) 232–242.
[56] D. Chen, J. Zhou, Q. Zhang, Effects of heating rate on slow pyrolysis behavior, kinetic parameters and products properties of moso bamboo, Bioresour. Technol. 169 (2014) 313–319.
[57] X. Yao, K. Xu, Y. Liang, Assessing the effects of different process parameters on the pyrolysis behaviors and thermal dynamics of corncob fractions, BioResources. 12 (2) (2017) 2748–2767.
[58] G. Wang, J. Zhang, J. Shao, Z. Liu, G. Zhang, T. Xu, J. Guo, H. Wang, R. Xu, H. Lin, Thermal behavior and kinetic analysis of co-combustion of waste biomass/low rank coal blends, Energ Conv Manag. 124 (2016) 414–426.
[59] Y. Xu, C. Zhang, J. Xia, Y. Duan, J. Yin, G. Chen, Experimental study on the comprehensive behavior of combustion for blended coals, Asia-Pac. J. Chem. Eng. 5 (3) (2010) 435–440.
[60] G. Wang, J. Zhang, J. Shao, S. Ren, Characterisation and model fitting kinetic analysis of coal/biomass co-combustion, Thermochim Acta 591 (2014) 68–74.
[61] J. Zheng, Y. Wang, W. Xu, Z. Gan, P. Li, J. Lv, GSSA: Pay attention to graph feature importance for GCN via statistical self-attention, Neurocomputing. 417 (2020) 458–470.
[62] W.-H. Chen, C.F. Eng, Y.-Y. Lin, Q.-V. Bach, Independent parallel pyrolysis kinetics of cellulose, hemicelluloses and lignin at various heating rates analyzed by evolutionary computation, Energ Conv Manag. 221 (2020) 113165.